Advances in Biochemistry & Applications in Medicine

Chapter 2

Functional Nanocrystals: Towards Biocompatibility, Nontoxicity and Biospecificity

Anielle Christine Almeida Silva[1]; Noelio Oliveira Dantas[1]; Marcelo José Barbosa Silva[2]; Mario Antônio Spanó[3]; Luiz Ricardo Goulart[4]*

[1]Laboratory of New Insulating and Semiconductor Materials (LNMIS), Physics Institute, Federal University of Uberlândia, Uberlândia, Minas Gerais, Brazil.

[2]Laboratory of Immunoparasitology, Institute of Biomedical Sciences, Federal University of Uberlândia, Uberlândia, Minas Gerais, Brazil.

[3]Laboratory of Mutagenesis, Institute of Genetics and Biochemistry, Federal University of Uberlândia, Uberlândia, Minas Gerais, Brazil.

[4]Laboratory of Nanobiotechnology, Institute of Genetics and Biochemistry, Federal University of Uberlândia, Uberlândia, Minas Gerais, Brazil.

***Correspondence to: Anielle Christine Almeida Silva**, Laboratory of New Insulating and Semiconductor Materials (LNMIS), Physics Institute, Federal University of Uberlândia, Uberlândia, Minas Gerais, Brazil*

Email: acalmeida@ufu.br

Abstract

The tunable surface chemistries have dramatically increased by expanding the structural arrangements of nanocrystals with many different strategies. Novel synthesis of functional colloidal nanocrystals has been developed over the past decade enabling the production of highly uniform and stable nanoparticles with important photonic characteristics. In this chapter, we will specifically comment on methodologies used in QDs syntheses that make nanocrystals highly biocompatible with important applications as luminescent probes. In addition, we will also discuss a new category of QDs named magic sized quantum dots (MSQDs), which present intense and broad luminescence rangeand greater size stability, turning them special tools for multiple biological applications in diagnosis, monitoring and therapy. Special emphasis will be placed on,safety, biocompatibility and biospecificity of nanomaterials, which are of great boncern as new techniques and novel nanocrystals emerge.

Almeida Silva AC

Keywords: nanocrystals; magic sized quantum dots; biocompatibility; genotoxicity; specific probe

1. Introduction

Quantum dots (QDs) of cadmium chalcogenides (CdSe, CdS and CdTe) have been used in several biological applications, since both absorption and emission spectra can be controlled as a function of size and shape [1-3]. As biological markers, QDs present several advantages over traditional organic fluorophores, such as long fluorescence lifetime(around 100 times greater) that allows to distinguish it from the background signalsobserved as autofluorescence-withshorter fluorescence absorption lifetime [4], greater photo-resistance and chroma-degradation, and a highlytunable fluorescence intensity [4,5]. However, QDs cytotoxicity is still a highly important subject due to its unpredicted behavior in the environment and within biological systems. We will specifically discuss, in this chapter, QDs syntheses methodologies, structural and physical characterizations, surface functionalization and bioconjugation, safety, biocompatibility and their applications

Zinc oxide (ZnO) and titanium dioxide (TiO$_2$) nanocrystals (NCs) have been widely used in sunscreens; therefore, biocompatibility and toxicity are inherently important subjects to investigate. ZnO is a group II-VI semiconductor with a hexagonal wurtzite crystal structure, with a broad energy band (3.37 eV), high bond energy (60 meV), and high thermal and mechanical stability at room temperature [6]. Furthermore, ZnO nanocrystals have antibacterial properties [7], and it has been added to several materials, including cotton fabrics, rubber and food packaging [8].

TiO$_2$ is semiconductor with bandgap around 3.0 eV (rutile) or 3.2 eV (anatase), with high photochemical stability [9]. When the size of the NCs is greatly reduced, the surface volume ratio increases and the quantum confinement effects may appear. In addition to size and shape, the crystalline phases of TiO$_2$ NCs also enable changes in physical properties. TiO$_2$ is a polymorphic material with three allotropic forms, namely anatase, brookite and rutile, with tetragonal (I4$_1$/amd), orthorhombic (Pbca) and tetragonal (P4$_2$/mnm) forms, respectively [10]. The anatase phase of TiO$_2$ NCs presents higher electron mobility, low dielectric constant, lower density, lower capacity to adsorb oxygen and higher degree of hydroxylation. The rutile phase has the highest thermodynamic stability at room temperature and pressure, but with higher levels of defects, besides being easier to be reduced. The brookite is the least studied crystalline phase due to the difficulties of production of a pure phase. This phase is often observed as a by-product when the precipitation is carried out in an acidic medium.

In view of these broad characteristics the systematic study of biocompatibility and genotoxicity in function of the size and crystalline phase of ZnO and TiO$_2$ NCs will also be approached in this chapter

www.openaccessebooks.com

2. Nanocrystals and quantum dots

The theory of crystal formation in solution is not a very simple matter and involves the analyses of several parameters used in the synthesis process. This section will cover an overview of crystal nucleation and growth processes.

The crystal growth occurs due to the crystallization of a homogeneous phase that begins and extends progressively from discrete centers distributed throughout the material. Thus, crystal formation occurs by sequential and periodic ordering of atoms in a standard structure and their growth due to the attachment of species present in the solution capable of reacting at the growth site, producing elements that will be part of the crystal structure. The crystal grows in the solution in order to decrease the free energy in the system as a result of two factors: achieving an orderly distribution of particles with maximum compensation of the chemical bonds and the mobility of the particles [11].

Figure 1 represents in (a) the most convenient energy position for grouping elementary entities that are at point 1, in which the least convenient is point 6. Small numbers indicate (in arbitrary units) the amount of energy released with the grouping of elementary entities in a given position (b) to the process of nutrition of the phases. Thus, nanocrystals are nanometric scale crystals.
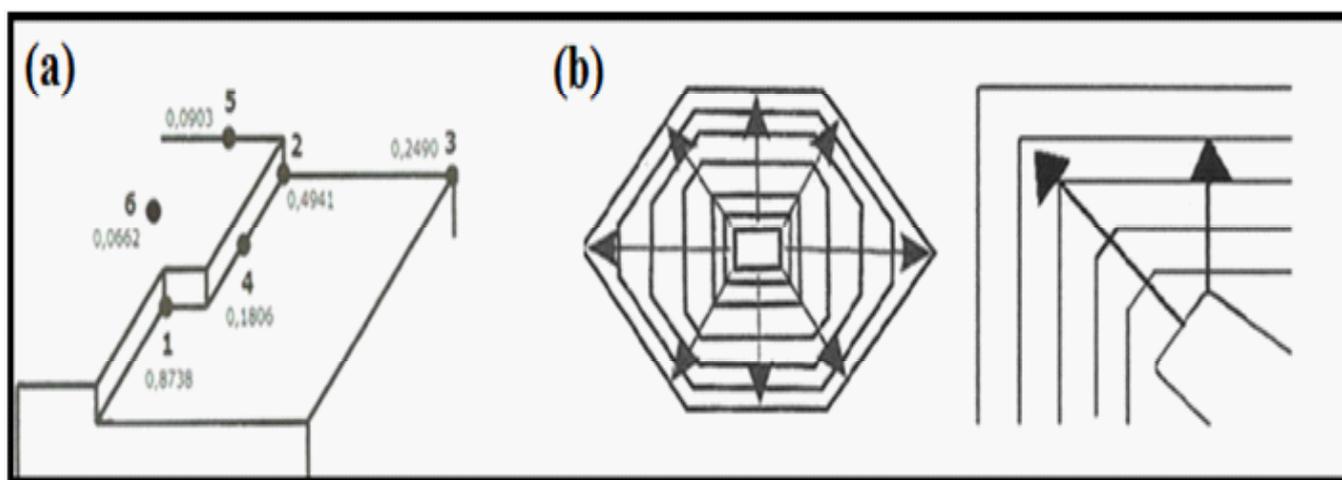

Figure 1.(a) Energy positions in the crystal; (b) Growing face of the crystal [11]

Nanocrystals can exhibit bulk and quantum confinement properties depending of the size and shape. Quantum dots (QDs) are nanocrystals that present quantum confinement in three dimensions. These dimensions must be larger than the lattice parameter and less or equal than Bohr radius of the corresponding bulk material. The Bohr radius of the exciton (r_{Bexc}) is the distance of the electron-hole pair, which is inversely proportional to the effective mass of the carriers (electrons and holes). The effective mass takes into account the mass of the carrier (electron or hole) plus the interactions between it and the ions of the crystalline lattice of the material [12]. Each material presents an effective mass of its carriers and consequently a given

Bohr radius, so depending on the material there may be different ranges of sizes with quantum confinement properties.

Figure 2 shows a schematic representation of spherical nanocrystals that presents quantum confinement properties (quantum dots) and bulk (without confinement), as well as the energy variation of the exciton with the size of the nanocrystal. When the radius of NCs is larger than the Bohr's exciton (r_{exc}) there is no quantum confinement property (bulk). In nanocrystals with bulk properties, energy levels are close to each other forming bands. Where as in quantum dots, the energy levels are quantized, resembling an artificial atom. Thus, in QDs the energy of the gap is altered with the size, allowing tuning its optical properties. The smaller the QDs size the higher the excitation energy.
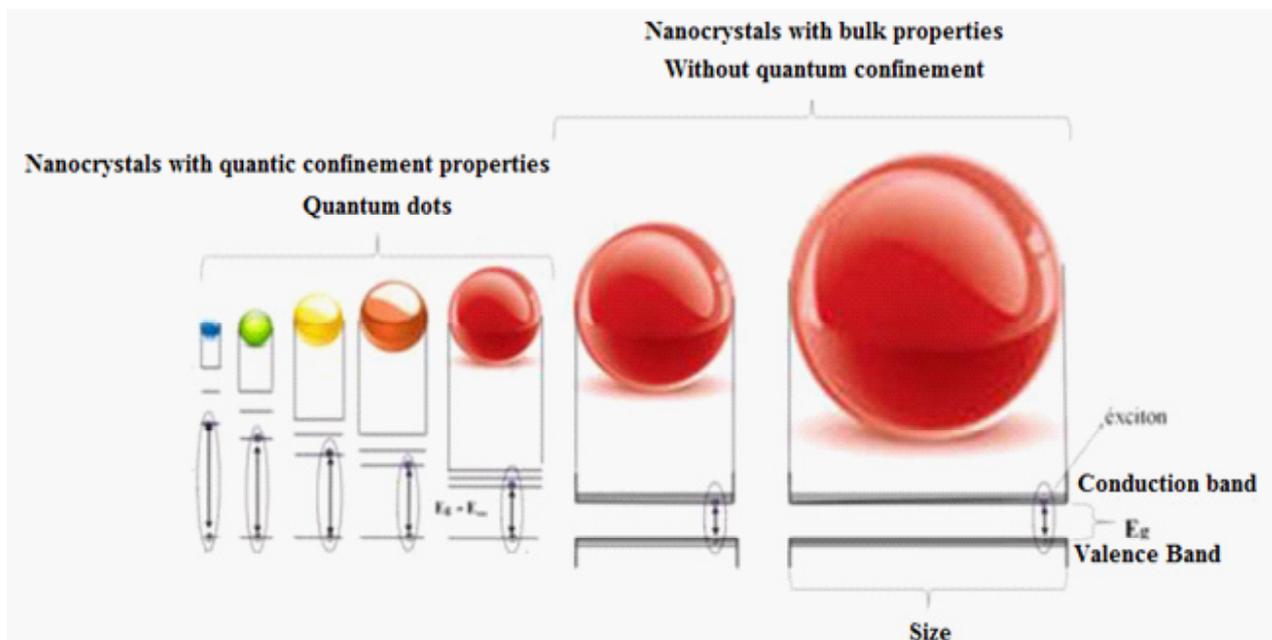

Figure 2: Variation of energy as a function of the size of the nanocrystals with and without quantum confinement properties [13].

The process of luminescence consists of three steps: excitation (creation electron-hole by an external source), thermalization (electrons and holes relax for the conduction band and valence bottom, respectively) and recombination (electrons and holes recombine producing an emission of photons).

Figure 3a illustrates the absorption process of a photon for the creation of the electron-hole followed by termination. The carriers position at the ends of the bands and the radiative recombine, in which a photon emission occurs in nanocrystals with properties of *bulk* and quantum confinement. It is observed that a decrease in size of QDs increases the transition energy between energy bands.

The quantum confinement properties present in QDs can be observed in the absorption and emission spectra, as shown in Figure 3b. In the case of CdSe, the indication of QDs formation is when the absorption band is at wave lengths shorter than the corresponding bulk

material (CdSe = 708 nm). The redshift between absorption and emission bands occurs due to decreased energy gap caused by the increase in size of QDs. Thus, based on the absorption and emission spectra, it is possible to monitor the growth kinetics.
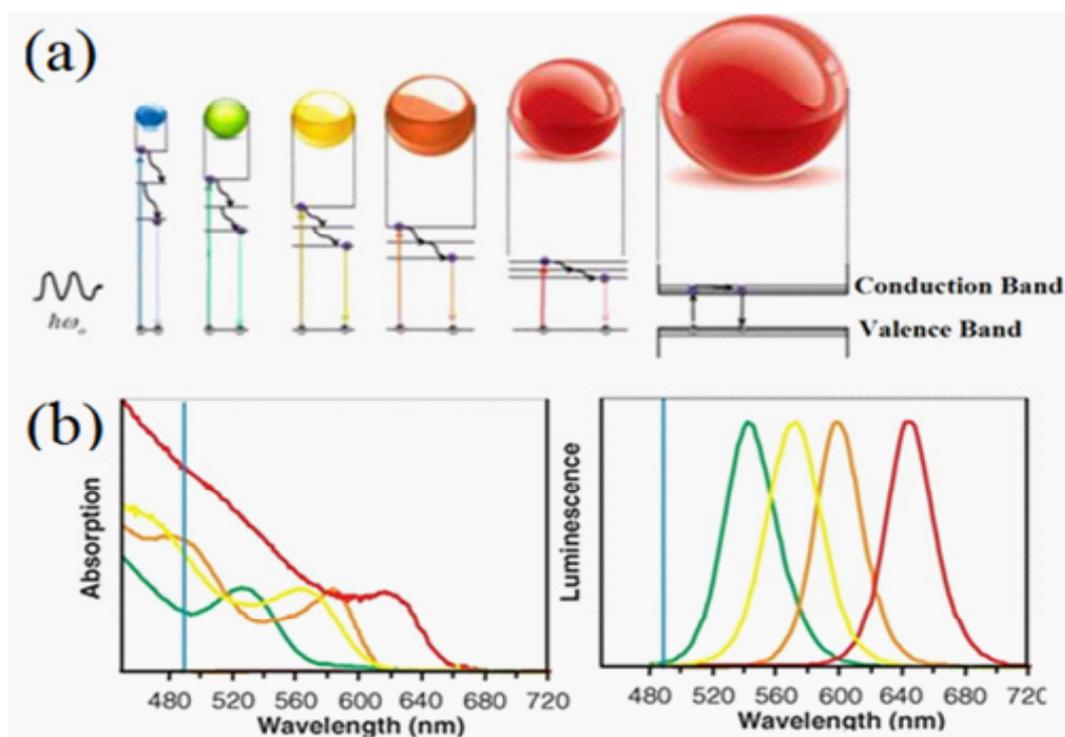

Figure 3: (a) Representative scheme of the absorption and emission process [13];(b) absorption and emission spectra of CdSe QDsof different sizes [14].

Magic-sized quantum dots (MSQDs) are quantum dots with extremely small sizes (<2 nm) and physical properties that are completely different from those presented by conventional QDs [15-17]. They present thermodynamically stable structures, wide luminescence range, great size stability over time, relatively narrow absorption spectra, and/or heterogenic growth [16,18-20]. In order to understand these structures Nguyen, Day and Pachtermade theoretical predictions of various types of CdSe MSQDs structures that are in agreement with the experimental results of the literature [21]. The term magic size is related to a (magic) number of atoms in the structure that makes MSQDs extremely stable. The wide luminescence spectrum occurs because MSQDs have internal atomic defects [20,22,23].

In addition to these characteristics, the MSQDs also present great stability of the luminescence within cells, allowing their use in assays that requires biological tracking and monitoring [24]. Examples of such property are shown by fluorescence microscopy images of CdSe MSQDs in HeLa cells in Figure 4, exposing cells for 24h**(a)** and 36h**(b)**.

3. Surface functionalization and bioconjugation

The functionalization process of QDs consists of coating the surface with organic molecules that carry specific chemical groups, such as carboxylic acid, thiol, amine, maleimide, aldehyde, epoxy, among others [25,26]. Such chemical groups in the QDs surface are used not

only to facilitate their dispersion in biological fluids, but also for conjugation with biological molecules, aiming their use as luminescent probes, as shown in Figure 5.
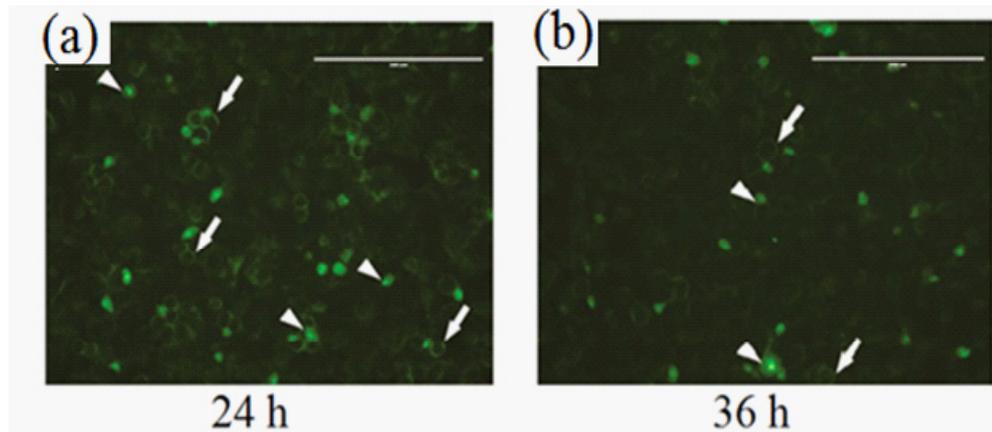

Figura 4: Fluorescence microscopy images of CdSe MSQDs in HeLa cells after (a)24h and(b) 36h [24]
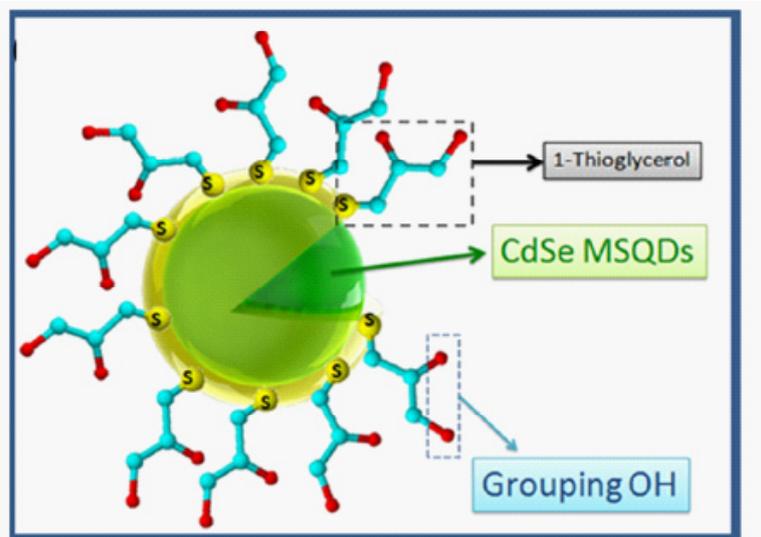

Figure 5: Representation of the functionalization nationalization process in QDs [24]

Another important process is the passivation, which is used to minimize the amount of electronic levels between the valence and conduction bands of the semiconductor, usually as a result of defects caused during the nanocrystal growth. These levels lead to non-radiative pathways by greatly suppressing the luminescence of nanocrystals. Therefore, after performing the passivation procedure, the defect levels decrease. This method resumes covering the core of the nanocrystal with an organic material or a semiconductor with energy gap larger than that of the nucleus as shown Figure 6. Therefore, this procedure is widely used in the synthesis of nanocrystals [27-29].
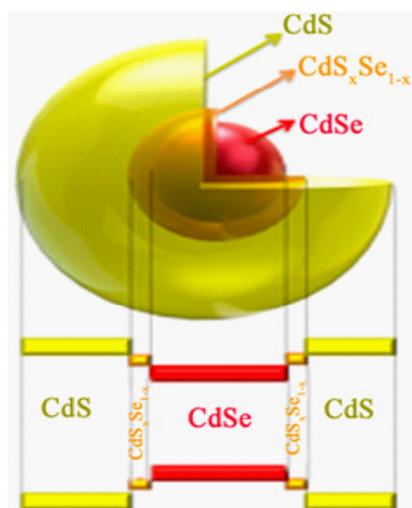
Figure 6: Representation of the process of inorganic passivation in QDs [31].

In a recent work, the passivation and functionalization processes have been performed in CdSe QDs, which have led to the formation of the CdS shell around the CdSe core of the QD as a function of the synthesis temperature [30] and the concentration of the stabilizer with external thiol grouping [31]. In addition, it was verified that the intensity of the luminescence is not proportional to the thickness of the shell. These methodologies were developed in order to increase the luminescence and biocompatibility of QDs, once cytotoxicity is related to the amount of $Cd2^+$ ions adsorbed on the surface of the CdSe QDs.

For biological and biomedical applications that use QDs as specific probes, the bioconjugation process is an important step. Depending on the specific chemical group in the surface of QDs, it is possible to attach a variety of biomolecules, including nucleic acids, proteins (e.g. avidin/streptavidin, albumin and antibodies), polysaccharides, and peptides. Therefore, the bioconjugation is performed after functionalization with the aim of coupling biological molecules to chemical bonds on QDs surface.

4. Biocompatibility of magic-sized quantum dots

Biocompatibility is the ability of nanomaterials in not causing toxicity or injury effects when in contact with live systems. Therefore, a biocompatible material must induce an appropriate host response [32,33]. The biocompatibility of materials is linked to their capacity of induce oxidative stress. An oxidative stress occurs when the production of oxidants surpass the antioxidant capacity in living cells. In this scenario, higher amounts of reactive oxygen species (ROS) and reactive nitrogen species (RNS) will exceed basal levels. These sub-products of oxygen and nitrogen species are implicated in a number of pathological conditions, such as cardiovascular and neurodegenerative diseases [34]. The excess of ROS and RNS also cause different modifications on DNA and proteins, and enhance lipid peroxidation that, in turn, decrease the antioxidant activity of enzymes as catalase, superoxide dismutase and glutathione peroxidase [35].

The size and shape of materials have an important effect on the secretion of oxidants [36]. The size effect on oxidative stress became mostly evident when tested materialsare particles. Some publications demonstrated that immune cells, such as macrophages, are typically capable of phagocytizing particles below 5 μm [37,38]. The phagocytosis elicits ROS production as an attempt to eliminate the internalized material. However, the greatest cellular effects are observed with sub-micrometer particles. It is important to point out that nanocrystals can directly stimulate ROS formation or trigger their production through activation or inhibition of enzymatic pathways. In *vivo* and in *vitro* studies demonstrated that the toxicity of nanocrystals is closely associated with intracellular ROS production [39]. Regarding QDs, several noxious effects have been reported *byin vitro* assays. Cell death induced by necrosis and apoptosis associated with oxidative stress response, and many associated cellular mechanisms, such as elevated cytochrome c and calcium, upregulation of Fas, a death receptor on the surface of the cell that leads to apoptosis have been reported [40-42].

Metalsare one of the components of biocompatible materials that arecapable of inducing oxidative stress. In many medical implants, metallic materials undergo electrochemical corrosion, which releases products of degradation at the implanted sites, causing the formation or ROS and RNS [43].The main reason of oxidative stress in cellular systemscaused by QDs is the presence of metal ions. Cadmium ions adsorbed on the surface of the QDs interact with oxygen molecules in cells causing significant toxicity [44].However, the reduced number of ions adsorbed on QDs surfaces and the diameters of core and shell may improve antioxidant properties by altering the uptake of QDs by cells, consequently diminishing the harmful effects of oxidative stress [41,44]. Based on this, it is important to analyze the biocompatibility of QDs with different sizes by evaluating their potential to induce harmful effects and oxidative stress.

One of the reasons of QDs harmful effects is the cadmium ions released from the inorganic core [42]. The cytotoxicity of $CdSe/CdS_xSe_{1-x}$ MSQDs functionalized with ahydroxyl group was investigated by fluorescence microscopy. Figure 7 shows the morphology of HeLa cells (A) incubated with CdSe MSQDs (B) and Etoposide (C). Acute cytotoxicity in HeLa cells was only observed after overnight exposure to Etoposide at 200 μM. HeLa cells incubated or not with CdSe MSQDs, observed by phase contrast microscopy, usuallyshow a thin and elongated form, which are homogeneously distributed throughout the culture and without cytotoxicity signs (Figure 5A and B). This specific result is due to the $CdSe_{1-x}S_x$ alloy at the shell protecting the CdSe core of the MSQDs, which prevents cadmium ion release,turning them more resistant to oxidation than other conventional QDs, from which reactions with oxygen usually cause $Cd2^+$ release from the core. On the other hand, the etoposide incubation led to various morphological abnormalities, as expected, such as reduced nuclear size, diverse degrees of chromatin condensation, cell shrinkage (round cells) and bleb formation on cell sur-

faces, which indicate terminal apoptosis (Fig. 7C). Therefore, CdSe/CdS$_x$Se$_{1-x}$ MSQDs did not alter the morphology of HeLa cells after 48-h incubation, suggesting no signs of cytotoxicity.
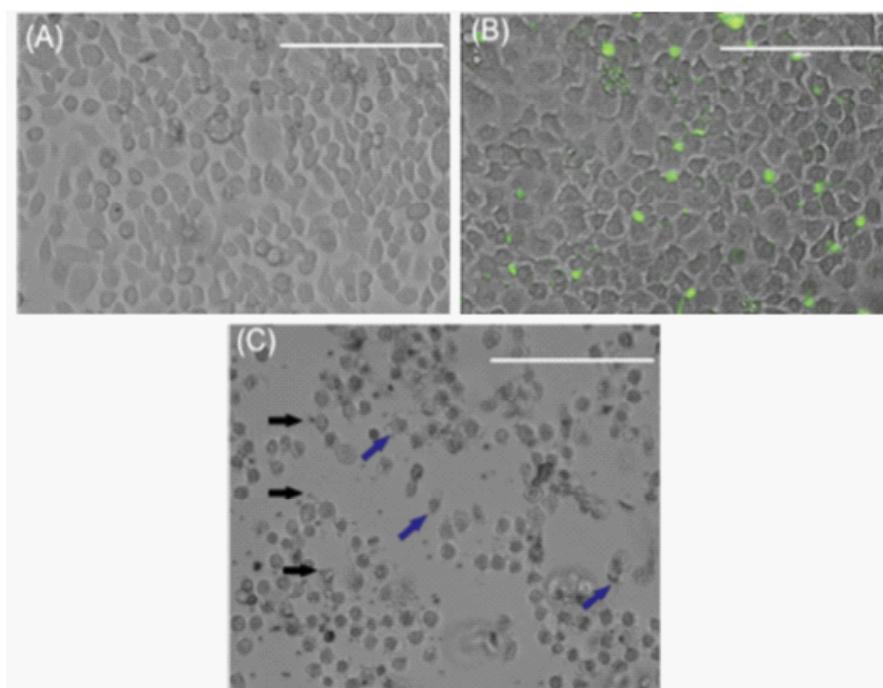

Figure 7: Morphological characterization of non-incubated (A) and incubated (B) HeLa cells submitted to MSQDs under phase contrast microscopy. Irregular shape and cellulardetachment (round cells) in etoposide treated cells are considered positive control of cytotoxicity (C). Black arrows indicate the formation of blebs on the cell surface as a result of the final death process. Blue arrows indicate the disruption of membrane cells. Scalebar = 200 μm [24].

In order to analyze what actually causes the cytotoxicity of cadmium chalcogenide MSQDs, we synthesized four samples with different concentrations of selenium during the synthesis, which directly affected the amount of Cd ions adsorbed on the surface of the MSQDs.

Figure 8a shows that levels of β-actin produced by cells were reduced after incubation as Se concentration increased [46]. Previously, it has been shown that the increased concentration of Cd ions adsorbed onto the MSQDs surface the higher the production of β-actin. The mRNA expression of themethallothionein gene(Figure 8b), an enzyme produced in the presence of metal ions, including cadmium [47,48], was lower when MSQDs presented less Cd ion concentration adsorbed at the MSQDs surface, suggesting that the cytotoxicity (Figure 8c) was due the concentration of Cd ions adsorbed on the surface of MSQDs; therefore, the more Se incorporated the smaller the harmful effects.
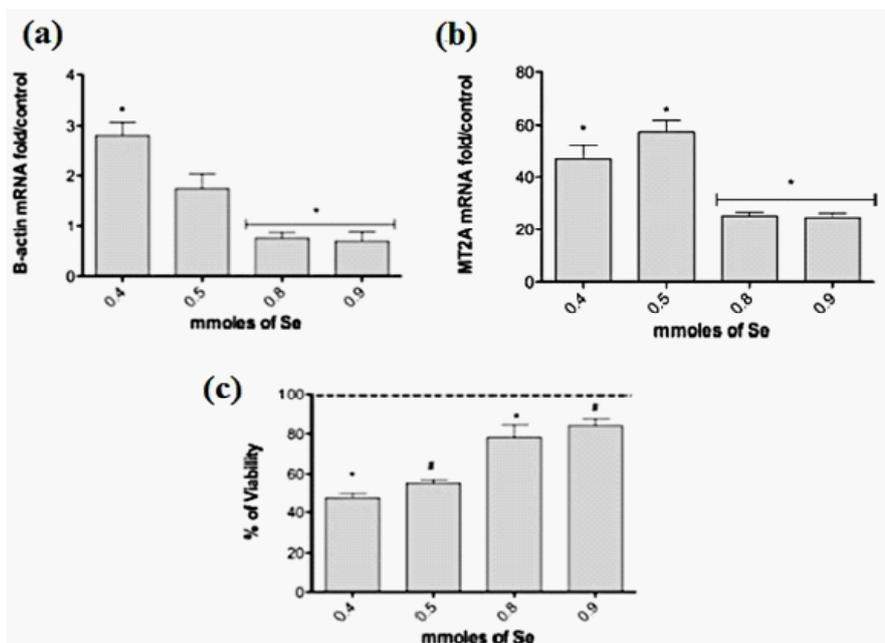
Figure 8. (a) MT2A expressions of HeLa cells exposed to CdSe MSQDs, synthesized at different Se concentrations, for 24 h. The mRNA expression was calculated as the ratio of fold to the control with POLR2A as an internal control. The results are expressed as means ±SE from two independent experiments. * represents $p <$ 0.05 comparing 0.8 and 0.9 with other groups. Cytotoxicity and β-actin mRNA expression of CdSe MSQDs synthesized at different Se concentrations (0.4−0.9 mmol) exposed to HeLa cells for 24 h. (b) The mRNA expression was calculated as the fold of the expression related with the control with the POLR2A expression as the internal control. The results are expressed as means ± SE from two independent experiments. * represents $p < 0.05$ comparing 0.8 and 0.9 with 0.4 Se. (c) Cell viability was calculated as a percentage of the viable untreated cells (control). The viability of the control cells was considered 100% (dotted line). The results are expressed as means ± SE from two independent experiments. *# represents $p < 0.05$ comparing 0.4 with 0.8 Se and 0.5 with 0.9 Se, respectively [46].

Figure 9 shows a simplified model of the CdSe MSQDs synthesized at different Se concentrations. As Se concentration increases, Cd^{2+} density on the surface of the CdSe MSQDs decreases. This consequently decreases concentrations of surface defect levels (SDL) (pending Cd^{2+} bonds) and increases the intensity of excitonic emissions (Eexc). Not only does the density of Cd^{2+} surface level defects diminish, but the size of the MSQDs increases slightly at higher Se concentrations.

The representative scheme presented in Figure 10, corresponding to the behavior of the fluorescence spectra, justifies the biological results, in which cytotoxicity decreases with increasing Se concentration and, consequently, a decrease in the density of free Cd^{2+} on the surface of CdSe MSQDs. Also, the induction of metallothionein 2A (MT2A) expression in CdSe MSQDs, mainly at 0.4 and 0.5 Se concentrations compared to the 0.8 and 0.9 concentrations, may reflect the greater Cd^{2+} presence at the surface in the smaller Se concentrations. At the same time, MT2A acts as a ROS scavenger, protecting the cell and reducing the cytotoxicity. Based on this data, a possible reason for the cytotoxicity of our CdSe MSQDs is the disruption of the transcriptional and posttranscriptional pathways of different proteins, including β-actin.
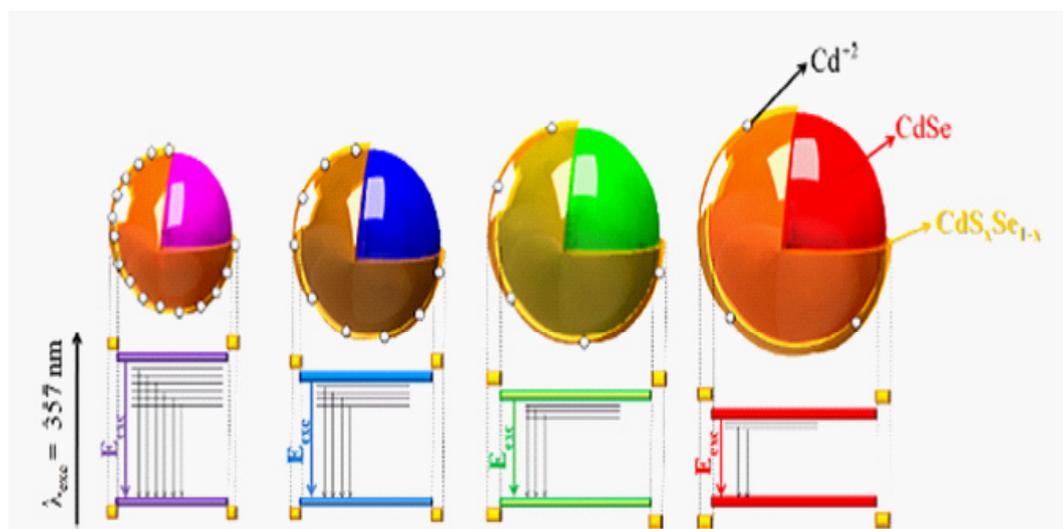
Figure 10: A simplified model of the CdSe MSQDs synthesized at different Se concentrations [46].

The cytotoxicity of CdSe/CdS$_x$Se$_{1-x}$/CdS MSQDs with external carboxylic chemical grouping was also investigated through MTT assays with the J774A.1 macrophage cell line (Figure 11A) and PBMCs from four healthy individuals under different concentrations of the MSQD (Figure 11B). The cell line incubated with different MSQDs concentrations did not show any significant cytotoxicity, except at concentrations ≥50 μg/mL during 24-h and 48-h incubation, in which the metabolic activity was significantly reduced. After 72-h incubation, a significant reduction of cell viability was also observed with MSQDs concentrations ≥10 μg/mL. PBMCs showed greater variations in cell viability without significant differences; however, with decreased viability as MSQDs concentration increased and during the time course of the stimulation assay.

In general, PBMCs showed greater viability than macrophages, and their variability was probably due to the heterogeneous cell population, which may be differentially affected by MSQDs. The cytotoxicity above 50 μg/mL may be justified by the aggregation of these QDs into organelles, such as mitochondria and lysosomes, altering their metabolic processes, and leading to a functional loss and death [44,49-51]. It is important to emphasize that such high concentrations of MSQDs are excessive for any cell line, and concentrations higher than 1 μg/mL are rarely used for specific applications.

The immunogenicity of MSQDs was analyzed by challenged PBMCs of healthy volunteers with 50 ng/mL MSQDs, the maximum concentration that did not show any cytotoxicity in PBMCs, as shown in Figure 12. There was no significant anti-inflammatory (IL-4, IL-10, TGF-β) (Figure 12, A) or proinflammatory (IL-2, IL-6, IL-8, TNF-alpha, IFN-gamma and IL-17A) (Figure 12, B) response, when compared to the negative control (untreated) in all incubation periods. TGF-β levels were relatively high in the immunogenicity assay, but cells treated with the MSQD were not significantly different from the control in none of the incubation periods, so we cannot infer that the CS-MSQD triggered TGF-β signaling.
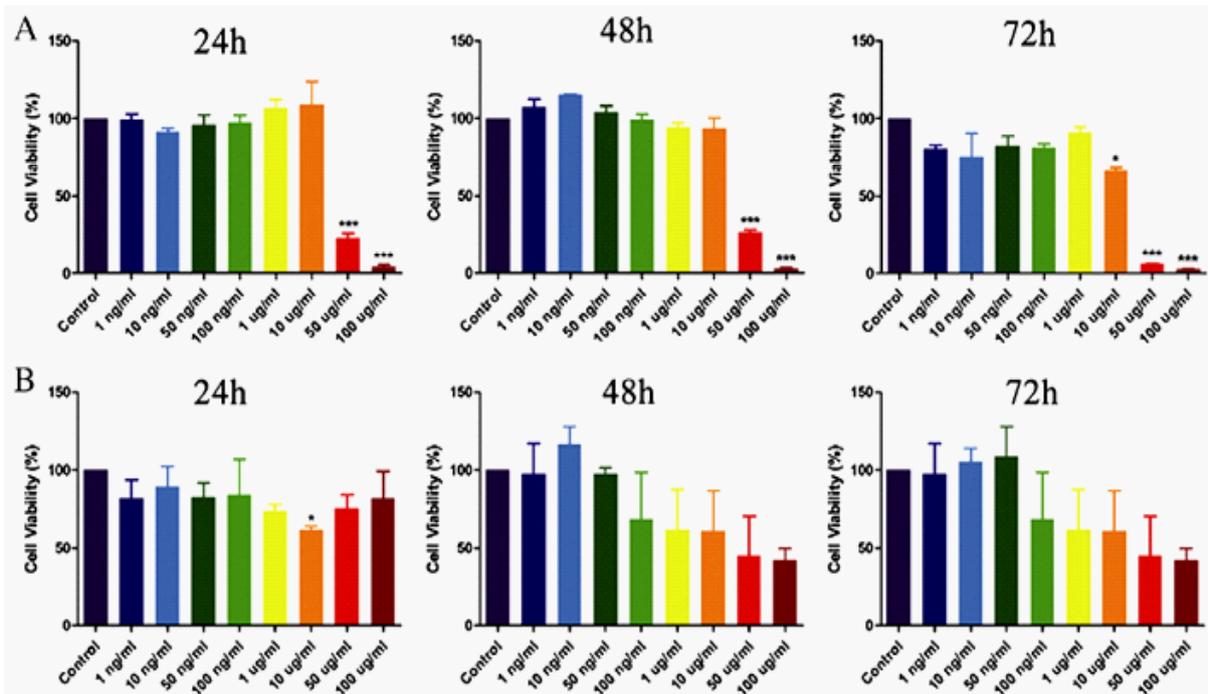
Figure 11: Cellular viability of the macrophage cell line J774A-1 (A) and PBMCs (B) from healthy individuals submitted to the MTT colorimetric assay after incubation with CdSe/CdS$_x$Se$_{1-x}$/CdS MSQDs. The MSQDs concentration ranged from 1 ng/mL to 100 μg/mL monitored from 24 to 120 h. MTT, 3-(4,5-dimethylthiazol-2-yl)-2,5-diphenyltetrazolium bromide. The results are expressed as means ± SD (standard deviation) from three independent experiments. *Statistical significance was considered when P < 0.05 in relation to control cultures (one-way ANOVA with post hoc Bonferroni's test) [52].
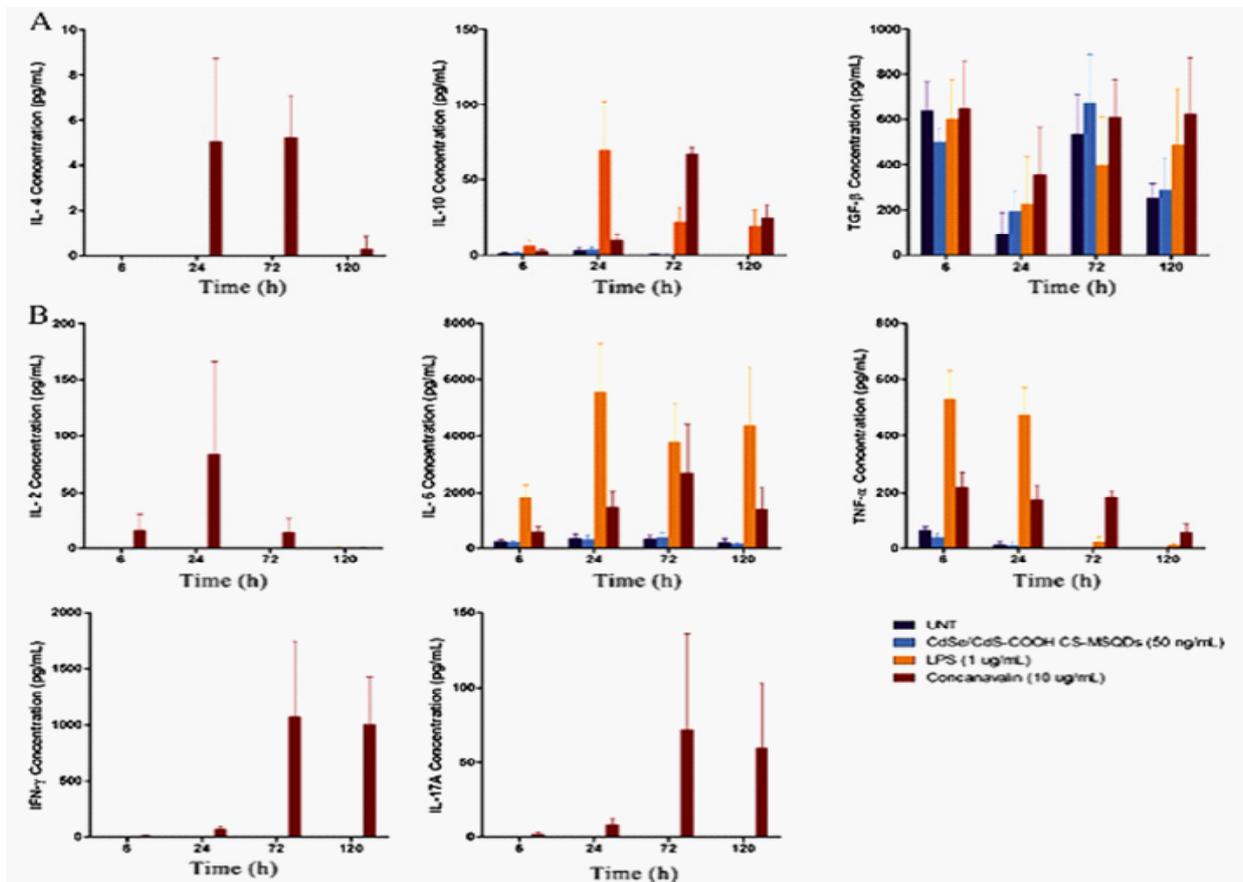
Figure 12: Th1/Th2/Th17 cytokines panel determination using cytometric bead array (CBA) assay of human PBMCs incubated with the CdSe/CdS$_x$Se$_{1-x}$/CdS MSQDs. Human PBMCs (N = 3) were treated with 50 ng/mL of MSQD for 6, 24, 72 and 120 h. Supernatants were harvested and assayed to determine the concentration of 8 different cytokines. Response profiles of pro- and anti-inflammatory cytokines were established. There were no statistical differences between QD stimulus and controls (untreated; UNT) (two-way ANOVA with post hoc Bonferroni's test). The lipopolysaccharide (1 μg/mL) and concanavalin (10 μg/mL) were used as positive controls of the reaction [52].

It is important to investigate the TGF-β signaling pathway due to its critical role in many biological processes, which is defined by the cell type and the micro environment [53,54], but while in infections it protects against excessive inflammation, it may also promote immune evasion and chronic infections. In autoimmune diseases, it leads to the loss of tolerance to self-antigens, and in cancer it acts as a potent inhibitor of cell proliferation and as tumor suppressor during tumorigenesis [55].

These pleiotropic and opposing roles of TGF-β may raise questions about the CS-MSQD applications in vivo either for diagnostics or drug delivery, especially for tumor imaging. However, in order to characterize the inflammatory or anti-inflammatory profiles of the immune response, one should consider common cytokines signatures and not a cytokine alone. In the present study, none of the evaluated cytokines showed a significant increase in the presence of the MSQD. So, the lack of immunogenicity corroborates the biocompatible nature of the MSQD. This is probably due to the ultra-small size, which may not be recognized by receptors, entering the cells by passive diffusion.

In summary, besides the toxicity analyses of new QDs, it is important to test their immunogenicity in order to prevent undesirable or unexpected response for *in vivo* applications.

5. Genotoxicity analyses of ZnO and Tio$_2$ nanocrystals

DNA damage can occur spontaneously through normal biological processes or asa result of direct or indirect interaction of DNA with chemical, physical or biological agents. The rapid development of nanotechnology allowed the increasing human environmental exposure to engineered nanocrystals in the form of industrial products such as dyes, paints, clothing, electronics, sunscreens, cosmetics, personal care products, food packaging, drug delivery systems, therapeutics, biosensors and others, generatingthe interest of researchers to investigate the potential hazards of NCs to DNA.

At present the genotoxic evaluation of NCs have been performed by means of different traditional genotoxicity tests, such as bacterial reverse mutation assay (Ames assay), *in vivo* and *in vitro* chromosomal aberration tests, in vivo comet assay, micronucleus test *in vivo* and *in vitro,* unscheduled DNA synthesis assay, somatic mutation and recombination test (SMART), among others [56-61].

In vivo studies offer many advantages, such as the study of the bioavailability of NCs to sensitive target cells and can increase the knowledge on the possible genotoxic potential risk associated with NCs exposure [62]. Nevertheless, the commonly used *in vivo* mammalian tests appear to be ill adapted to tackle the large compound sets involved, due to throughput, cost, and ethical issues. Non-mammalian animals, such as the common fruit fly Drosophila melanogaster are good candidates for the development of high-throughput genotoxicity tests due to their quick reproductive cycles, greater ethical acceptance, and smaller infrastructure needs [63], as it has a mammalian-like enzymatic system that allows the breakdown of xeno-biotic agents. Many basic biological, physiological, and neurological properties are conserved between mammals and D. melanogaster, and nearly 75% of human disease-causing genes are believed to have a functional homolog in the fly [64]. In addition to presenting highly reli-able and reproducible results, it allows to quantify the recombinogenic activity against the mutagenic activity of different compounds and mixtures [65]. Recently, a review article on Drosophotoxicology Chifiriuc et al. [66] has been published as an emerging research area for assessing nanocrystals interaction with living organisms. Additionally,it has also been pre-sented the suitability of D. melanogaster as an in vivo model to determine potential side effects of nanomaterials [67].

On the other hand, the toxicological relevance of in vitro assays as the micronucleus(MN) test is due to the fact that it is a multi-target genotoxic endpoint that assesses not only theclas-togenic and aneugenic events, but also some epigenetic effects. It is simple to score, accurate, applicable to different cell types, predictive for cancer, amenable for automation, and easily measured in experimental both *in vitro* and *in vivo* systems [68]. MN is a small nuclei-like structure enveloped by a nuclear membrane, located in the cytoplasm outside of the main daughter nuclei, which represent either a whole lagging chromosome (resulting of an aneu-genic event leading to chromosome loss) or an acentric fragment of a chromosome (resulting of clastogenic event) that was retained in anaphase and not incorporated into one of the daugh-ter nuclei during cell division [69,70]. The *in vitro* Cytokinesis Block Micronucleus (CBMN), established inhuman peripheral blood lymphocytes has several advantages, such as the speed and easiness, no requirement for metaphase cells, and reliable identification of cells that have completed only one nuclear division.

For these reasons, we highlight the Drosophila wing somatic mutation and recombina-tion test (SMART), also known as the wing spot test, and the CBMN assay as potential meth-odologies to assess the genotoxic potential of NCs.

5.1 Somatic mutation and recombination test in D. melanogaster

The SMART provides a rapid means to assess the potential of a chemical to induce loss of heterozygosity (LOH) resulting from gene mutation, chromosomal rearrangement, chromo-

some breakage, or chromosome loss. This bioassay makes use of the wing-cell recessive markers *multiple wing hairs (mwh, 3–0.3)* and *flare (flr3, 3–38.8),* located at the tip and roughly in the middle of the left arm of chromosome 3, respectively. The LOH leads to uncovering and expression of the recessive marker gene(s) in the larval imaginal disk cells. They give rise to clones of mutant cells showing up as mosaic spots on the wings [71,72]. Two crosses are usually carried out to produce the experimental larval progeny: [1] ST cross, flr³/In(3LR)TM3, ri pᵖsep l(3)89Aa bx³⁴ᵉ e Bdˢ females crossed with mwh males [73,74];[2] HB cross, ORR; flr³/In(3LR)TM3, ri pᵖsep l(3)89Aa bx3⁴ᵉ e Bdˢ females crossed with *mwh* males [75]. The latter cross is characterized by improved sensitivity to a number of promutagens and procarcinogens owing to high levels of constitutively expressed cytochromes P450. Both crosses produce two types of progeny: (i) marker-heterozygous (MH) flies; (ii) balancer-heterozygous (BH) flies, as shown in Figure 13.

In MH individuals, single spots (*mwh or flr)* can be produced either by point mutation, certain types of chromosome breakage event (deletion) or by mitotic recombination. However, we cannot tell how much each mechanism contributes to the total of spots recovered. On the other hand, the presence of twin spots proves that mitotic recombination is induced, as these spots result from mitotic crossing-over between the *flr* locus and the centromere. Figure 14presents a twin spot found in the blade of *Drosophila* wing showing normal and mutants flare and multiple wing hairs.
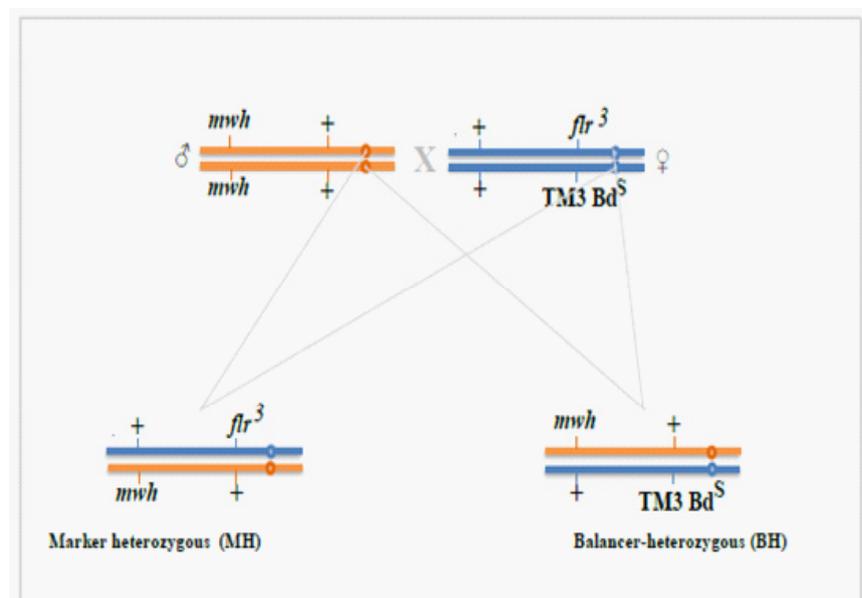

Figure 13: Standard (ST) cross: mwhmales crossed with flr3/In(3LR)TM3, ri pp sep l(3)89Aa bx34e e BdS-females producing two types of progeny: marker-heterozygous(MH) flies and balancer-heterozygous (BH) flies.
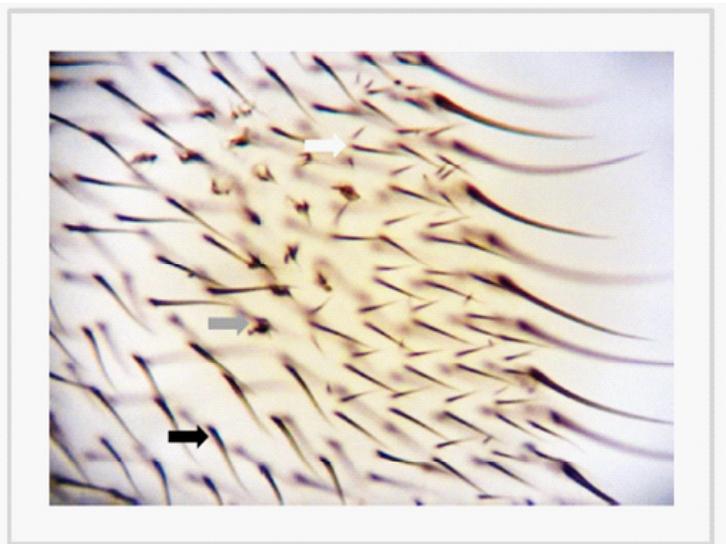
Figure 14: Twin spot found in the blade of Drosophila wing showing normal hair (black arrow), flare hair (gray arrow), and multiple wing hairs (white arrow).

In BH individuals, the flr marker is absent. The spots that can be recovered are therefore mwh single spots. All recombination events are suppressed or eliminated owing to inversion heterozygosity brought about by the presence of the multiply inverted balancer chromosome. As a rule, therefore, the frequencies of mwh clones observed on the wings of BH flies are always lower than those observed on the wings of MH flies [73,76]. Many hundreds of chemicals have already been tested using SMART, including NCs [60,62,72,77-79].

The wing SMART in *D. melanogaster* has been widely used to assess genotoxic potential of different chemicals compounds, including NCs. Here we only present some selected results obtained with ZnO NCs and TiO$_2$ NCs.

The mutagenic and recombinogenic potential of an amorphous and ZnONCs (20 nm) using both crosses of the wing SMART of D. *melanogaster* has been evaluated [60]. Third instar larvae were fed chronically (approximately 48 h) with four different concentrations (ranging from 1.56 to 12.50 mM). In the ST cross, the amorphous and ZnO NCs (20 nm) were not mutagenic. Nevertheless, MH individuals from the HB cross that were treated with amorphous (6.25 mM) and ZnO NCs (12.50 mM) displayed a significant increased number of mutant spots when compared with the negative control. The increase in mutant spots observed in *D. melanogaster* was generated due to mitotic recombination, rather than mutational events. Our results suggest that ZnO mutagenicity can be related to particle size and shape. As ZnO NCs had a uniform feature with an average size of 20 nm, it could enter the cell homogeneously and cause mutagenicity at higher concentrations. On the other hand, as the amorphous ZnO comprises a mixture of structures of different shapes and sizes, its mutagenicity could be variable, according to the size and shape of the crystals and its ability to enter the cell. Consequently, mutagenic effects related to the dose could not be expected.

In agreement with the previous results, it has also been described a lack of genotoxic ac-

tivity of different concentrations (6, 12, 18 or 24 mM) of ZnO NCs and ZnO bulk assayed with the ST cross of the *Drosophila* wing-spot test [80]. Nevertheless, when these authors tested both particles in haemolymph cells of *Drosophila* by the comet assay, a significant increase in DNA damage was observed at the higher dose applied of ZnO NCs. The authors concluded that the genotoxic potential of ZnO NCs could be considered low or weak because it promotes only primary genetic damage restricted to high-dose exposures, which can be easily repaired.

On the other hand, ZnO NCs with an average size of 50 nm, assayed with the ST cross showed a significant increase in the frequency of mutant clones in the flies exposed to the concentration of 1.2 mg/mL [81].

The genotoxic effects of 3.4 and 6.2 nm TiO_2 anatase NCs (A3.4 and A6.2) and 78.0 nm predominantly TiO_2 rutile NCs (R78.0) through the *Drosophila* wing SMART were also evaluated [79]. Third instar larvae obtained from standard (ST) or high bioactivation (HB) crosses were treated with a solution containing TiO_2 (A3.4, A6.2 or R78.0) NCs at concentrations ranging from 1.5625 to 100.0 mM. In the ST cross, no mutagenic effects were observed. However, in the HB cross, TiO_2A3.4 NCs were mutagenic at 1.5625 and 3.125 mM, while theR78.0 NCs increased mutant spots at all concentrations tested except 3.125 mM. Only the smallest anatase TiO_2 NCs induced mutagenic effects. Therefore, both anatase and rutile TiO_2 NCs induced mutagenicity.

Negative results in the ST cross had already been observed previouslywith TiO_2 NCs (2.3 nm) at concentration ranging from 0.1 to 10 mM [78] and with TiO_2 anatase NCs (<25 nm particle size, surface area 45–50 m2/g, 99.7% purity) as well as their TiO_2anatase bulk form (TiO_2 bulk, 45 μm, 99% purity) [77]. Third instar larvae were fed with both compounds at different concentrations (0.08, 0.40, 0.80 and 1.60 mg/mL, respectively). None of the concentrations of TiO_2 NCs and TiO_2 bulk induced significant increases in the frequency of mutant spots. Nevertheless, in this study, the authors evaluated the same concentrations of both nano- and bulk forms of TiO_2 with the comet assay in Drosophilahemocytes. TiO_2 NCs at concentrations ranging from 0.40 to 1.60 mg/mL induced a significant increase in DNA damage, with a direct dose-response pattern.

5.2 Cytokinesis-block micronucleus (CBMN) assay

The *in vitro* Cytokinesis Block Micronucleus (CBMN) Assay is one of the standard cytogenetic tools used widely as a screening *in vitro* test for structural or numerical chromosomal anomalies induced by clastogenic or aneugenic agents (''spindle poisoning'') [82]. This technique consists in adding to cell cultures cytochalasin-B, an inhibitor of the mitotic spindle that prevents cytokinesis, producing binucleated cells, allowing a more accurate MN score and excluding the dividing cells from the non-dividing cells to enhance the reliability by reducing the incidence of false positive data [83].

Figure 15 shows a binucleated cell with a MN. The CBMN assay has been used to evaluate clastogenic and aneugenic effects of different compounds, including NCs [60,78,79,84].
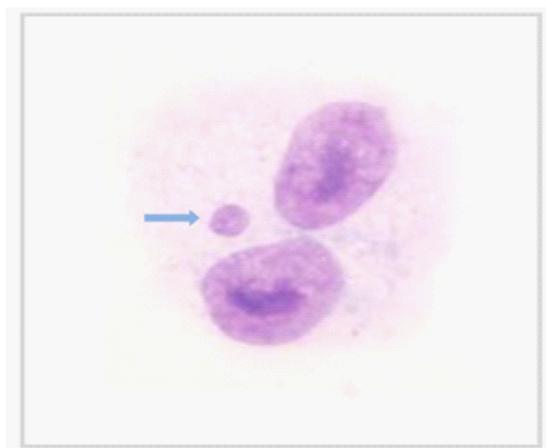

Figure 15: Optical microphotography of V79 binucleated cells with micronucleus (arrow) (Giemsa; total increase: 1000×).

Here, we will only present selected results obtained with ZnO NCs and TiO$_2$ NCs using an *in vitro* CBMN Assay. The genotoxic potential of ZnO NCs of 20 nm using the Chinese hamster lung fibroblast V79 cells has been evaluated [60], and results demonstrated that were not dose-dependent and indicated that only higher concentrations of ZnO NCs were toxic and able to induce genotoxicity in V79 cells.

In agreement with the previous data, significant increase of MN was observed in human epithelial HEp-2 cell line treated with ZnO NCs at high concentrations (50 and 100 μg/ml) (Osman et al., 2010); in A549 human lung carcinoma cells treated with 50 μg/ml ZnONC [85]; in human peripheral blood mononuclear cells treated with ZnO NCs at a concentration of 45 μg/ml [86];and human peripheral lymphocytes treated with ZnO (diameter of 45 nm and fragment size of 450 nm) at 10 and 15μg/ml [88].

The genotoxic effects of 3.4 and 6.2 nm anatase TiO$_2$ NCs and 78.0 nm predominantly rutile TiO$_2$ NCs were also evaluated through CBMN assay using V79 cells treated with 30, 60 or 120 mM anatase 3.4 or A6.2 TiO$_2$, and 976.5, 1953.0 or 3906.0 mM rutile 78.0 TiO$_2$ [79]. Only the smallest anatase (3.4 nm) TiO$_2$ NCs significantly increased the frequency of MN at the highest concentration (120 mM), showing a genotoxic effect. No significant differences in MN induction were observed in the groups treated with 30 and 60 mM A3.4 TiO$_2$ when compared to negative control ($p>0.05$). The results also demonstrated lack of genotoxic (clastogenic/aneugenic) effects for A6.2 and R78.0 TiO$_2$ at all concentrations tested.

Similar results were observed else where [89], in which the genotoxicity of three reference TiO$_2$ nanomaterials (NM) was also investigated in human bronchial epithelial BEAS 2B cells. The BEAS 2B cells were submitted to NM100 (anatase, 50–150 nm), NM101 (anatase, 5–8 nm) and NM103 (rutile, 20–28 nm) TiO$_2$ dispersions at 1, 5 or 15 μg/ml (0.2–3.2 μg/cm2)

for 48h, and increase MN was observed only by the rutile NM103 in the lowest concentrations tested (1 and 5 µg/ml).

We propose the *Drosophila* wing SMART and the CBMN assays as *in vivo* and *in vitro* systems, respectively, to screen NCs for potential genotoxicity, mutagenicity and recombinogenicity. Nevertheless, due to the contradictory results found in the literature, further research is necessary to clarify the NCs action mechanisms, highlighting the importance of using more than one genetic end-point.

6. Biocompatible luminescent probes using magic-sized quantum dots

In a recent work, the CdSe/CdS$_x$Se$_{1-x}$/CdS-COOH MSQDs has been successfully conjugated to a specific antibody for breast cancer aiming their use as biological probe, as shown Figure 16. Additionally, it has been shown that this MSQDs presented low cytotoxicity and no immune response, enabling their use for *in vivo* applications.
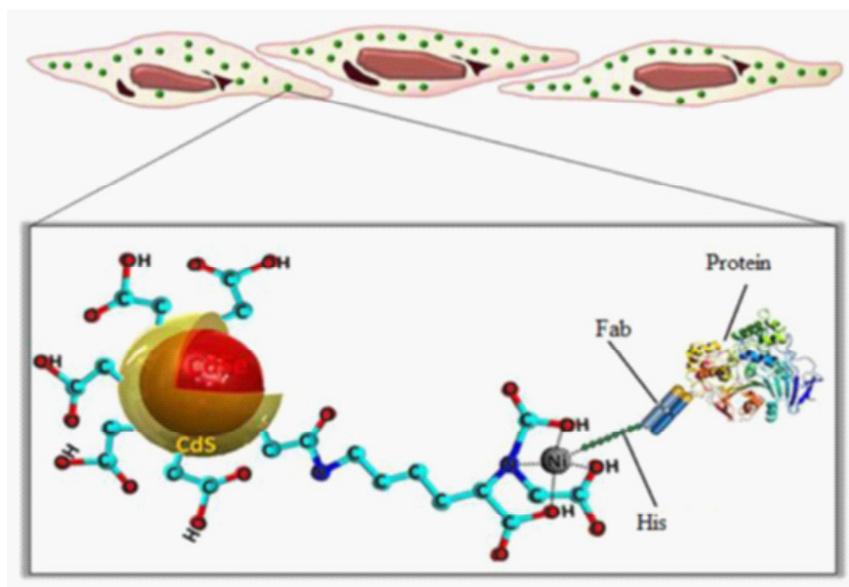

Figure 16: Representation of bioconjugation process performed [52].

The bioconjugation procedure of the MSQD-COOH with an Fab antibody by means of the compound containing nickel ion (precursor nickel chloride $NiCl_2$) together with nitrilo-acetic acid (NTA • Ni^{2+}) is described in Figure 17. Thus, the development of CdSe/CdS$_x$Se$_{1-x}$/CdS MSQDs complex with NTA•Ni^{2+} moieties exposed at the surface, which are capable of specifically recognizing histidine-tagged Fab antibodies, was used to detect breast cancer cells by immuno fluorescence.
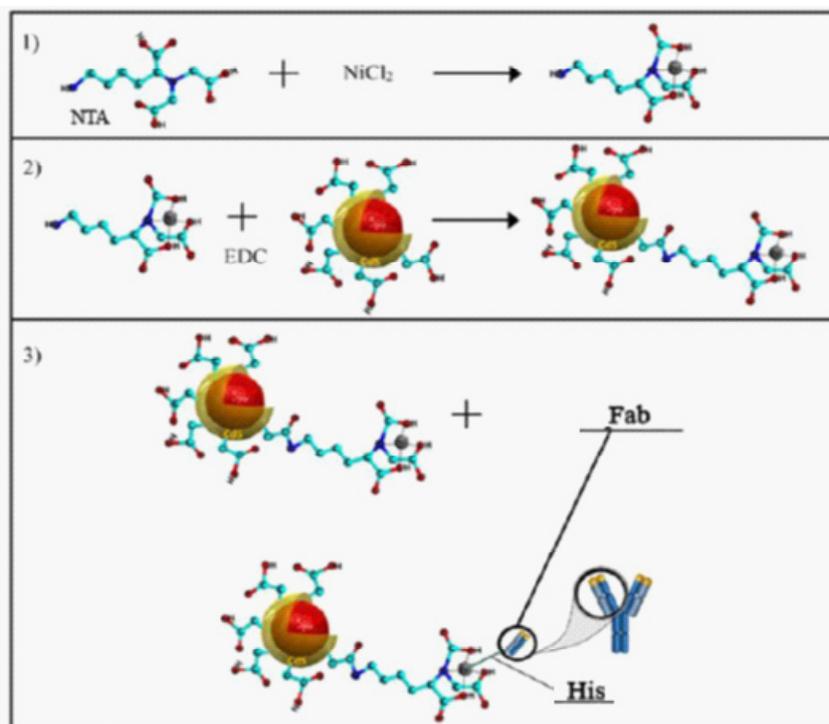
Figure 17: Schematic representation of the reactions to bioconjugateCdSe/CdS$_x$Se$_{1-x}$/CdSMSQDs to an antibody specific for breast cancer. MSQDs were functionalized with the NTA • Ni^{2+} complex, which interacted with the histidine tail of the Fab antibody.

In order to confirm the functionalization of the MSQDs-COOH with an NTA • Ni^{2+} complex, and the bioconjugation with the Fab antibody, the Fourier Transform Infrared (FT-IR) spectroscopy was used, as shown in Figure 18.

The spectrum of MSQDs observed at the broad band 3423–3292 cm−1 shows the specific characteristics of OH group and adsorbing water(Figure 18). The presence of bands at 1280, 1556, 1357 cm^{-1} and 1713–1602 cm^{-1} are associated with vibrations of hydroxyl, antisymmetric vC=O, asymmetric vCOO− and symmetric vCOO$^-$ groups, respectively [90]. These peaks confirmed that MSQDs are functionalized with carboxyl group at the surface. Moreover, in the spectrum of MSQDs also showed that the peak at 2600 cm^{-1} of stretching modes of S–H bonding disappeared, confirming the covalent bond formation between S of the stabilizer molecule and cadmium ions (Cd^{2+}) of the MSQDs, forming a shell of CdS [31]. Furthermore, the spectra of the MSQDs showed bands around 609 cm^{-1} and 1622 cm−1 that reinforce the formation of the CdS shell around the CdSe MSQDs [31]. The shell prevents Cd^{2+} release from the CdSe core and makes the MSQDs less cytotoxic, which is confirmed by tests with specific cellular metabolic activity under stimuli of MSQD.

The FT-IR spectrum of the MSQDs coupled with antibody presented pronounced bands of amide I and II vibrational stretches at 1645 and 1555 cm^{-1} (squared box), respectively, and shifts in the N–H stretching region (3500-3000 cm^{-1}) [91]. This demonstrates that the MSQDs are covalently attached to NTA • Ni^{2+} moieties through an organic linkage and not through nonspecific binding interaction, and coupling of CS-MSQD with Fab antibody was carried out

through the interaction of Ni^{2+} with the histidine tag present in the antibody [92], coordinated by imidazole binding, confirmingbthe conjugation as demonstrated in Figure 17 [93]. It was also noted that the vibrational modes corresponding to Fab antibody (region from 550-1550 cm^{-1}) remained intact, demonstrating that coupling did not affect the 3D structure of the conjugated Fab antibody, and did not alter the specificity, the cytosolic conformational epitope of cytokeratin 10 (CK-10) [94].
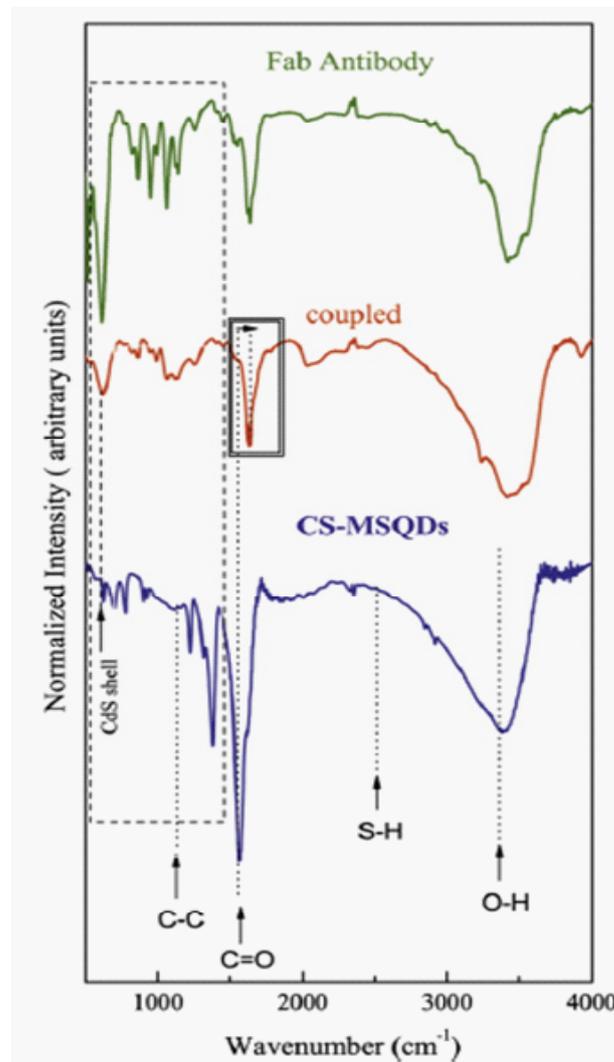

Figure 18: FT-IR spectra Fab antibody and of the CdSe/CdS$_x$Se$_{1-x}$/CdSMSQDs pre- and post-bioconjugation [52].

It is important to check the bioconjugation also by means of biological assays. Thus, imaging analysis were performed to test the efficiency of MSQDs coupled to a specific breast cancer Fab antibody in an immuno cytochemistry assay. Figure 19 shows a highfluorescence intensity demonstrating that the MSQDs were efficiently conjugated to Fab antibodies with high specificity to breast cancer cells when compared with controls (non-labeled MSQDs). The cell auto-fluorescence in the control (Figure 15A) is similar to that observed in Figure 15B, which was expected because MSQDs in Figure 15B were washed off, and only few random spots could be seen. The higher magnification setting in Figure 15A was used to demonstrate the auto-fluorescence behavior of cells without MSQDs. However, the most striking difference is shown in Figure 15C, where specific immunoagglutination has occurred.
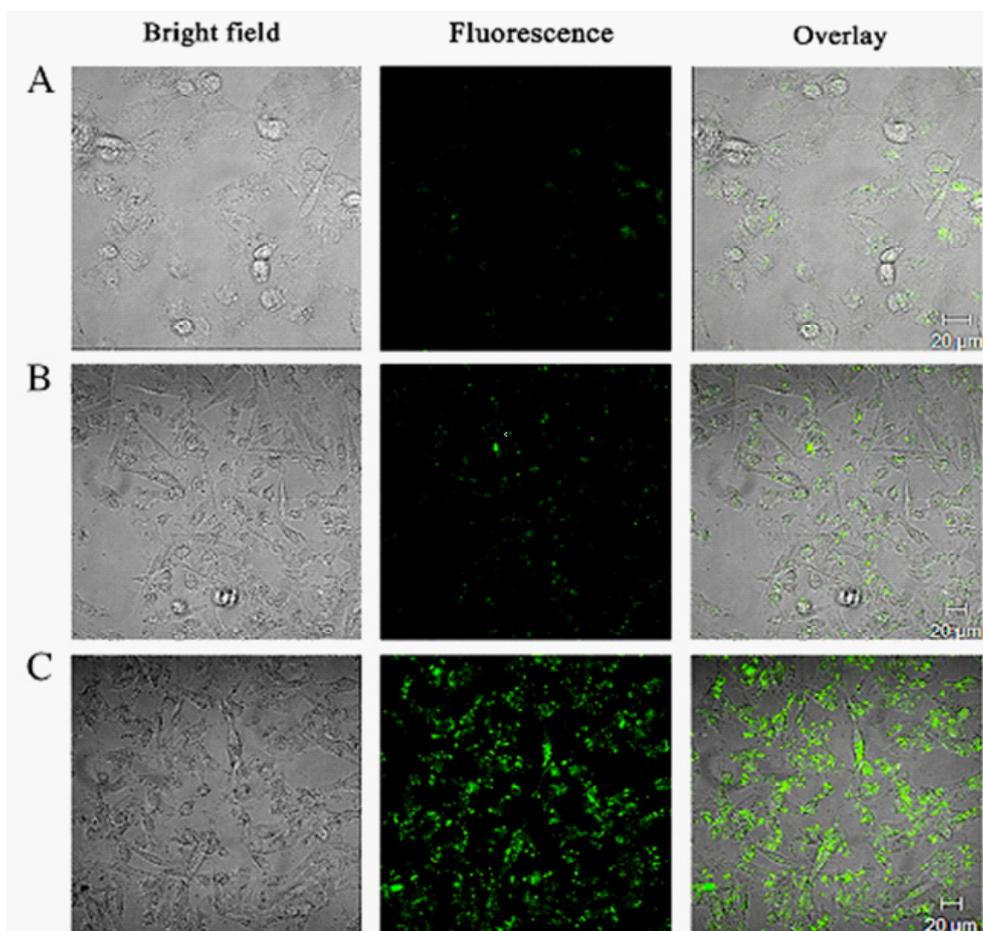
Figure 19: Specific cytosolic labeling of the breast cancer (BC) cell line MDA-MB-231 with CdSe/CdS$_x$Se$_{1-x}$/CdS MSQDs conjugated with a specific BC Fab antibody analyzed by confocal microscopy. Cells were incubated with MSQDs for 1 h. (A) MDA-MB cells (control); (B) MDA-MB cells incubated with MSQDs; (C) MSQDs conjugated to Fab antibody. Images obtained in Zeiss LSM 510 Meta Confocal Microscope with laser emission 530 nm (green channel) [52].

The CS-MSQD presents high fluorescence stability, low toxicity, no immunogenicity, and biocompatibility, demonstrating to be a powerful tool for diagnostic and imaging techniques. These highly desirable characteristics may also present great potential for drug delivery, which must still be demonstrated.

7. References

1. Jennings, T.L., Triulzi, R.C., Tao, G., et al. (2011) Simplistic attachment and multispectral imaging with semiconductor nanocrystals. Sensors (Basel)., 11 (11), 10557–70.

2. Zhang, H., Yee, D., and Wang, C. (2008) Quantum dots for cancer diagnosis and therapy: biological and clinical perspectives. Nanomedicine (Lond)., 3, 83–91.

3. Zhang, X., Guo, Q., and Cui, D. (2009) Recent advances in nanotechnology applied to biosensors. Sensors, 9 (2), 1033–1053.

4. Resch-Genger, U., Grabolle, M., Cavaliere-Jaricot, S., et al. (2008) Quantum dots versus organic dyes as fluorescent labels. Nat. Methods, 5 (9), 763–775.

5. Deerinck, T.J. (2008) The application of fluorescent quantum dots to confocal, multiphoton, and electron microscopic

imaging. Toxicol. Pathol., 36 (1), 112–6.

6. Kolodziejczak-Radzimska, A., and Jesionowski, T. (2014) Zinc oxide-from synthesis to application: A review. Materials (Basel)., 7 (4), 2833–2881.

7. Padmavathy, N., and Vijayaraghavan, R. (2008) Enhanced bioactivity of ZnO nanoparticles—an antimicrobial study. Sci. Technol. Adv. Mater., 9 (3), 35004.

8. Saito, M. (1993) Antibacterial, Deodorizing, and UV Absorbing Materials Obtained with Zinc Oxide (ZnO) Coated Fabrics. J. Ind. Text., 23 (2), 150–164.

9. Kamat, P. V. (2012) TiO 2 nanostructures: Recent physical chemistry advances. J. Phys. Chem. C, 116 (22), 11849–11851.

10. Reyes-Coronado, D., Rodríguez-Gattorno, G., Espinosa-Pesqueira, M.E., et al. (2008) Phase-pure TiO(2) nanoparticles: anatase, brookite and rutile. Nanotechnology, 19 (14), 145605.

11. Alan Holden, P.M. (1982) Crystals and Crystal Growing. 318.

12. Kittel, C. (1968) Introduction to Solid State Physics, John Wiley and Sons.

13. Silva, A.C.A. (2014) Semiconductor Quantum Dots Synthesized by Aqueous Colloidal Solutions: Studies and Nanobiotechnology Applications.

14. Michalet, X., Pinaud, F.F., Bentolila, L. a, et al. (2005) Quantum dots for live cells, in vivo imaging, and diagnostics. Science, 307 (5709), 538–44.

15. Xia, Y.-S., and Zhu, C.-Q. (2008) Aqueous synthesis of luminescent magic sized CdSe nanoclusters. Mater. Lett., 62 (14), 2103–2105.

16. Zou, Q.D., Dongmei, L., Jingjing, C., et al. (2007) Facile synthesis of magic-sized CdSe and CdTe nanocrystals with tunable existence periods. Nanotechnology, 18 (40), 405603.

17. Neeleshwar, S., Chen, C.L., Tsai, C.B., et al. (2005) Size-dependent properties of CdSe quantum dots. Phys. Rev. B, 71 (20), 201307.

18. Riehle, F.S., Bienert, R., Thomann, R., and Urban, G.A. (2009) Blue Luminescence and Superstructures from Magic Size Clusters of CdSe. Nano Lett., 9 (2), 514–518.

19. Babentsov, V.N. (2006) Defects with deep donor and acceptor levels in nanocrystals of CdTe and CdSe. Semicond. Physics, Quantum Electron. Optoelectron., 9 (3), 94–98.

20. Dukes, A.D., McBride, J.R., and Rosenthal, S.J. (2010) Synthesis of Magic-Sized CdSe and CdTe Nanocrystals with Diisooctylphosphinic Acid. Chem. Mater., 22 (23), 6402–6408.

21. Nguyen, K.A., Day, P.N., and Pachter, R. (2010) Understanding Structural and Optical Properties of Nanoscale CdSe Magic-Size Quantum Dots: Insight from Computational Prediction. J. Phys. Chem. C, 114 (39), 16197–16209.

22. Bowers, M.J., McBride, J.R., and Rosenthal, S.J. (2005) White-light emission from magic-sized cadmium selenide nanocrystals. J Am Chem Soc, 127, 15378–15379.

23. McBride, J.R., Dukes, A.D., Schreuder, M. a, and Rosenthal, S.J. (2010) On Ultrasmall Nanocrystals. Chem. Phys. Lett., 498 (1–3), 1–9.

24. Silva, A.C.A., Deus, S.L.V. de, Silva, M.J.B., and Dantas, N.O. (2014) Highly stable luminescence of CdSe magic-sized quantum dots in HeLa cells. Sensors Actuators B Chem., 191, 108–114.

25. Mazumder, S., Dey, R., Mitra, M.K., et al. (2009) Review: Biofunctionalized Quantum Dots in Biology and Medi-

cine. J. Nanomater., 2009, 1–17.

26. Sperling, R. a, and Parak, W.J. (2010) Surface modification, functionalization and bioconjugation of colloidal inorganic nanoparticles. Philos. Trans. A. Math. Phys. Eng. Sci., 368 (1915), 1333–83.

27. Zeng, R., Zhang, T., Liu, J., et al. (2009) Aqueous synthesis of type-II CdTe/CdSe core-shell quantum dots for fluorescent probe labeling tumor cells. Nanotechnology, 20 (9), 95102.

28. Xiao, Q., and Xiao, C. (2008) Synthesis and photoluminescence of water-soluble Mn:ZnS/ZnS core/shell quantum dots using nucleation-doping strategy. Opt. Mater. (Amst)., 31 (2), 455–460.

29. Silva, A.C.A., Neto, E.S.F., Silva, W., et al. (2013) Modified Phonon Confinement Model and Its Application to CdSe/CdS Core−Shell Magic-Sized Quantum Dots Synthesized in Aqueous Solution by a New Route. J. Phys. Chem. C, 117, 1904−1914.

30. Silva, A.C.A., Neto, E.S.F., da Silva, S.W., et al. (2013) Modified Phonon Confinement Model and Its Application to CdSe/CdS Core–Shell Magic-Sized Quantum Dots Synthesized in Aqueous Solution by a New Route. J. Phys. Chem. C, 117 (4), 1904–1914.

31. Silva, A.C.A., da Silva, S.W., Morais, P.C., and Dantas, N.O. (2014) Shell Thickness Modulation in Ultrasmall CdSe/CdSxSe1–x/CdS Core/Shell Quantum Dots via 1-Thioglycerol. ACS Nano, 8 (2), 1913–1922.

32. Williams, D.F. (2008) On the mechanisms of biocompatibility. Biomaterials, 29 (20), 2941–2953.

33. Williams, D. (2003) Revisiting the definition of biocompatibility. Med. Device Technol., 14 (8), 10–13.

34. Mouthuy, P.-A., Snelling, S.J.B., Dakin, S.G., et al. (2016) Biocompatibility of implantable materials: An oxidative stress viewpoint. Biomaterials, 109, 55–68.

35. Tsaryk, R., Peters, K., Unger, R.E., et al. (2013) The Role of Oxidative Stress in the Response of Endothelial Cells to Metals, in Biologically Responsive Biomaterials for Tissue Engineering (eds.Antoniac, I.), Springer New York, New York, NY, pp. 65–88.

36. Chih-Chang Chu, J. Anthony von Fraunhofer, H.P.G. (1999) Wound Closure Biomaterials and Devices. CRC Press, 11 (3), 226.

37. Eliaz, N. (2012) Degradation of implant materials. Degrad. Implant Mater., 1–516.

38. Sheikh, Z., Brooks, J.P., Barzilay, O., et al. (2015) Macrophages, Foreign Body Giant Cells and Their Response to Implantable Biomaterials. Mater. , 8 (9).

39. Khanna, P., Ong, C., Bay, B., and Baeg, G. (2015) Nanotoxicity: An Interplay of Oxidative Stress, Inflammation and Cell Death. Nanomaterials, 5 (3), 1163–1180.

40. Lovrić, J., Cho, S.J., Winnik, F.M., and Maysinger, D. (2005) Unmodified Cadmium Telluride Quantum Dots Induce Reactive Oxygen Species Formation Leading to Multiple Organelle Damage and Cell Death. Chem. Biol., 12 (11), 1227–1234.

41. Yan, M., Zhang, Y., Xu, K., et al. (2011) An in vitro study of vascular endothelial toxicity of CdTe quantum dots. Toxicology, 282 (3), 94–103.

42. Choi, A.O., Cho, S.J., Desbarats, J., et al. (2007) Quantum dot-induced cell death involves Fas upregulation and lipid peroxidation in human neuroblastoma cells. J. Nanobiotechnology, 5, 1.

43. Sansone, V., Pagani, D., and Melato, M. (2013) The effects on bone cells of metal ions released from orthopaedic implants. A review. Clin. Cases Miner. Bone Metab., 10 (1), 34–40.

44. Li, K.G., Chen, J.T., Bai, S.S., et al. (2009) Intracellular oxidative stress and cadmium ions release induce cytotoxic-

ity of unmodified cadmium sulfide quantum dots. Toxicol Vitr., 23, 1007–1013.

45. Derfus, A.M., Chan, W.C.W., and Bhatia, S.N. (2004) Probing the Cytotoxicity of Semiconductor Quantum Dots. Nano Lett., 4 (1), 11–18.

46. Silva, A.C.A., Silva, M.J.B., Da Luz, F.A.C., et al. (2014) Controlling the cytotoxicity of CdSe magic-sized quantum dots as a function of surface defect density. Nano Lett., 14 (9), 5452–5457.

47. Nath, R., Kambadur, R., Gulati, S., et al. (1988) Molecular aspects, physiological function, and clinical significance of metallothioneins. Crit. Rev. Food Sci. Nutr., 27 (1), 41–85.

48. Tmejova, K., Hynek, D., Kopel, P., et al. (2014) Study of metallothionein–quantum dots interactions. Colloids Surfaces B Biointerfaces, 117, 534–537.

49. Chen, N., He, Y., Su, Y., et al. (2012) The cytotoxicity of cadmium-based quantum dots. Biomaterials, 33 (5), 1238–44.

50. Su, Y., He, Y., Lu, H., et al. (2009) The cytotoxicity of cadmium based, aqueous phase - Synthesized, quantum dots and its modulation by surface coating. Biomaterials, 30 (1), 19–25.

51. Hardman, R. (2006) A toxicologic review of quantum dots: Toxicity depends on physicochemical and environmental factors. Environ. Health Perspect., 114 (2), 165–172.

52. Silva, A.C.A., Freschi, A.P.P., Rodrigues, C.M., et al. (2016) Biological analysis and imaging applications of CdSe/CdSxSe1−x/CdS core–shell magic-sized quantum dot. Nanomedicine Nanotechnology, Biol. Med., 12 (5), 1421–1430.

53. Fleisch, M.C., Maxwell, C.A., and Barcellos-Hoff, M.H. (2006) The pleiotropic roles of transforming growth factor beta in homeostasis and carcinogenesis of endocrine organs. Endocr. Relat. Cancer, 13 (2), 379–400.

54. Ruscetti, F.W., and Bartelmez, S.H. (2001) Transforming growth factor beta, pleiotropic regulator of hematopoietic stem cells: potential physiological and clinical relevance. Int. J. Hematol., 74 (1), 18–25.

55. Mantel, P., and Schmidt-Weber, C.B. (2011) Transforming growth factor-Beta: recent advances on its role in immune tolerance. Methods Mol. Biol., 677, 303–38.

56. Kwon, J.Y., Lee, S.Y., Koedrith, P., et al. (2014) Lack of genotoxic potential of ZnO nanoparticles in in vitro and in vivo tests. Mutat. Res. - Genet. Toxicol. Environ. Mutagen., 761, 1–9.

57. Pal, A., Alam, S., Mittal, S., et al. (2016) UVB irradiation-enhanced zinc oxide nanoparticles-induced DNA damage and cell death in mouse skin. Mutat. Res. - Genet. Toxicol. Environ. Mutagen., 807, 15–24.

58. Pan, X., Redding, J.E., Wiley, P.A., et al. (2010) Mutagenicity evaluation of metal oxide nanoparticles by the bacterial reverse mutation assay. Chemosphere, 79 (1), 113–116.

59. Panda, K.K., Achary, V.M.M., Phaomie, G., et al. (2016) Polyvinyl polypyrrolidone attenuates genotoxicity of silver nanoparticles synthesized via green route, tested in Lathyrus sativus L. root bioassay. Mutat. Res. - Genet. Toxicol. Environ. Mutagen., 806, 11–23.

60. Reis, É. de M., Rezende, A.A.A. de, Santos, D.V., et al. (2015) Assessment of the genotoxic potential of two zinc oxide sources (amorphous and nanoparticles) using the in vitro micronucleus test and the in vivo wing somatic mutation and recombination test. Food Chem. Toxicol., 84, 55–63.

61. Alaraby, M., Hernández, A., and Marcos, R. (2017) Copper oxide nanoparticles and copper sulphate act as antigenotoxic agents in drosophila melanogaster. Environ. Mol. Mutagen., 58 (1), 46–55.

62. Demir, E., Vales, G., Kaya, B., et al. (2011) Genotoxic analysis of silver nanoparticles in Drosophila. Nanotoxicology, 5 (September), 417–424.

63. Sung-Jun, H. (2015) High-throughput, in vivo genotoxicity testing: an automated readout system for the Somatic Mutation And Recombination Test (SMART).

64. Pandey, U.B., and Nichols, C.D. (2011) Human disease models in Drosophila melanogaster and the role of the fly in therapeutic drug discovery. Pharmacol. Rev., 63 (2), 411–436.

65. Machado, N.M., de Rezende, A.A.A., Nepomuceno, J.C., et al. (2016) Evaluation of mutagenic, recombinogenic and carcinogenic potential of (+)-usnic acid in somatic cells of Drosophila melanogaster. Food Chem. Toxicol., 96, 226–233.

66. Chifiriuc, M.C., Ratiu, A.C., Popa, M., and Ecovoiu, A. Al (2016) Drosophotoxicology: An emerging research area for assessing nanoparticles interaction with living organisms. Int. J. Mol. Sci., 17 (2).

67. Alaraby, M., Annangi, B., Marcos, R., and Hernández, A. (2016) Drosophila melanogaster as a suitable in vivo model to determine potential side effects of nanomaterials: A review. J. Toxicol. Environ. Heal. Part B, 19 (2), 65–104.

68. Kirsch-Volders, M., Decordier, I., Elhajouji, A., et al. (2011) In vitro genotoxicity testing using the micronucleus assay in cell lines, human lymphocytes and 3D human skin models. Mutagenesis, 26 (1), 177–184.

69. Fenech, M. (2007) Cytokinesis-block micronucleus cytome assay. Nat. Protoc., 2 (5), 1084–1104.

70. Pejchal, J., Vasilieva, V., Hristozova, M., et al. (2011) Cytokinesis-Block Micronucleus (Cbmn) Assay / Cbmn Cytome Assay in Human Lymphocytes After in Vitro Irradiation and Its Use in Biodosimetry. 80 (October 2015), 28–37.

71. Spanó, M. a, Frei, H., Würgler, F.E., and Graf, U. (2001) Recombinagenic activity of four compounds in the standard and high bioactivation crosses of Drosophila melanogaster in the wing spot test. Mutagenesis, 16 (5), 385–394.

72. de Andrade, H.H., Reguly, M.L., and Lehmann, M. (2004) Wing Somatic Mutation and Recombination Test, in Drosophila Cytogenetics Protocols (eds.Henderson, D.S.), Humana Press, Totowa, NJ, pp. 389–412.

73. Graf, U., W??rgler, F.E., Katz, A.J., et al. (1984) Somatic mutation and recombination test in Drosophila melanogaster. Environ. Mutagen., 6 (2), 153–188.

74. Graf, U., Frei, H., Kägi, A., et al. (1989) Thirty compounds tested in the Drosophila wing spot test. Mutat. Res. Toxicol., 222 (4), 359–373.

75. Graf, U., and van Schaik, N. (1992) Improved high bioactivation cross for the wing somatic mutation and recombination test in Drosophila melanogaster. Mutat. Res. Mutagen. Relat. Subj., 271 (1), 59–67.

76. Frei, H., and Würgler, F.E. (1996) Induction of somatic mutation and recombination by four inhibitors of eukaryotic topoisomerases assayed in the wing spot test of Drosophila melanogaster. Mutagenesis, 11 (4), 315–325.

77. Carmona, E.R., Escobar, B., Vales, G., and Marcos, R. (2015) Genotoxic testing of titanium dioxide anatase nanoparticles using the wing-spot test and the comet assay in Drosophila. Mutat. Res. - Genet. Toxicol. Environ. Mutagen., 778, 12–21.

78. Demir, E., Burgucu, D., Turna, F., et al. (2013) Determination of TiO2, ZrO2, and Al2O3 nanoparticles on genotoxic responses in human peripheral blood lymphocytes and cultured embyronic kidney cells. J. Toxicol. Environ. Health. A, 76 (16), 990–1002.

79. Reis, É. de M., Rezende, A.A.A. de, Oliveira, P.F. de, et al. (2016) Evaluation of titanium dioxide nanocrystal-induced genotoxicity by the cytokinesis-block micronucleus assay and the Drosophila wing spot test. Food Chem. Toxicol., 96, 309–319.

80. Carmona, E.R., Inostroza-Blancheteau, C., Rubio, L., and Marcos, R. (2016) Genotoxic and oxidative stress potential of nanosized and bulk zinc oxide particles in Drosophila melanogaster. Toxicol. Ind. Health, 32 (12), 1987–2001.

81. Lences, C., Cardozo, T., Carli, R. de, et al. (2016) AVALIAÇÃO, IN VIVO, DA TOXICIDADE GENÉTICA DE

NANOPARTÍCULAS DE ÓXIDO DE ZINCO. Rev. iniciação Cient. da UFBRA, 14, 1–5.

82. Fenech, M., and Morley, A.A. (1985) Measurement of micronuclei in lymphocytes. Mutat. Res. Mutagen. Relat. Subj., 147 (1–2), 29–36.

83. Deepa Parvathi, V., and Rajagopal, K. (2014) Nanotoxicology testing: Potential of Drosophila in toxicity assessment of nanomaterials. Int. J. Nanosci. Nanotechnol., 5 (1), 25–35.

84. Tavares, A.M., Louro, H., Antunes, S., et al. (2014) Genotoxicity evaluation of nanosized titanium dioxide, synthetic amorphous silica and multi-walled carbon nanotubes in human lymphocytes. Toxicol. Vitr., 28 (1), 60–69.

85. Osman, I.F., Baumgartner, A., Cemeli, E., et al. (2010) Genotoxicity and cytotoxicity of zinc oxide and titanium dioxide in HEp-2 cells. Nanomedicine, 5 (8), 1193–203.

86. Corradi, S., Gonzalez, L., Thomassen, L.C.J., et al. (2012) Influence of serum on in situ proliferation and genotoxicity in A549 human lung cells exposed to nanomaterials. Mutat. Res. - Genet. Toxicol. Environ. Mutagen., 745 (1–2), 21–27.

87. Bhattacharya, D., Santra, C.R., Ghosh, A.N., and Karmakar, P. (2014) Differential toxicity of rod and spherical zinc oxide nanoparticles on human peripheral blood mononuclear cells. J. Biomed. Nanotechnol., 10 (4), 707–716.

88. Gümüş, D., Berber, A.A., Ada, K., and Aksoy, H. (2014) In vitro genotoxic effects of ZnO nanomaterials in human peripheral lymphocytes. Cytotechnology, 66 (2), 317–325.

89. Bucchianico, S. Di, Cappellini, F., Bihanic, F. Le, et al. (2016) Genotoxicity of TiO 2 nanoparticles assessed by mini-gel comet assay and micronucleus scoring with flow cytometry. Mutagenesis, 1–11.

90. Pérez-Donoso, J.M., Monrás, J.P., Bravo, D., et al. (2012) Biomimetic, mild chemical synthesis of Cdte-GSH quantum dots with improved biocompatibility. PLoS One, 7 (1).

91. Pan, B., Cui, D., He, R., et al. (2006) Covalent attachment of quantum dot on carbon nanotubes. Chem. Phys. Lett., 417 (4–6), 419–424.

92. Hainfeld, J.F., Liu, W., Halsey, C.M.R., et al. (1999) Ni–NTA–Gold Clusters Target His-Tagged Proteins. J. Struct. Biol., 127 (2), 185–198.

93. Gupta, M., Caniard, A., Touceda-Varela, Á., et al. (2008) Nitrilotriacetic Acid-Derivatized Quantum Dots for Simple Purification and Site-Selective Fluorescent Labeling of Active Proteins in a Single Step. Bioconjug. Chem., 19 (10), 1964–1967.

94. Araújo, T.G., Paiva, C.E., Rocha, R.M., et al. (2017) A novel highly reactive Fab antibody for breast cancer tissue diagnostics and staging also discriminates a subset of good prognostic triple-negative breast cancers. Cancer Lett., 343 (2), 275–285.